Metallomacrocycle (MacM) Complex with Cyanide as Bridged Ligand: Electronic Structures of $[MacMCN]_n$

FERNANDO MENDIZABAL,[1] CLAUDIO OLEA-AZAR[2]

[1]*Departamento de Química, Facultad de Ciencias, Universidad de Chile, Casilla 653-Santiago, Chile*
[2]*Departamento de Química Inorgánica y Analítica, Facultad de Ciencias Químicas y Farmacéuticas, Universidad de Chile, Casilla 233, Santiago 1, Chile*

ABSTRACT: The electronic structures of complexes and one-dimensional metallomacrocycles with cyanide as bridged ligand, such as $[MacM(CN)_2]^-$ and $[MacM(CN)]_n$ [Mac = phthalocyanine, tetrabenzoporphyrine; M = Co(III), Rh(III)] have been investigated using density functional theory. The results of this study show that the intrinsic semiconductivity properties depend on the frontier bands. The valence band is composed by the π-macrocycle orbital. The conduction band for the cobalt polymers is a mixture of orbitals between this metal and the cyanide ligand along of the stacking direction. However, in the rhodium polymers such a band is exclusively composed of the π^* system of the macrocycles.

Key words: metallomacrocycles complexes and polymers; electronic properties; density functional calculations

Introduction

The semiconducting properties in quasi-one-dimensional macrocycle transition metal complexes linked by linear bridging ligand (L)–$[MacM(L)]_n$ have been determined [1–14]. Commonly the macrocycles (Mac) used in these complexes are phathalocyanine (Pc), tetrabenzoporphyrine (TBP), 1,2- and 2,3-naphthalocyanine (1,2- and 2,3-Nc), and others. The transition metals are Fe, Ru, Os, and Co; and other metals in the oxidation state +II were taken as central metals. The ligands (L) are linear π-electron-containing organic molecules bonded to the metal atom [15–26].

The electrical properties exhibited by these systems have attracted much attention [27, 28]. For instance, the bridged transition metal compounds are fairly stable polymers that exhibit intrinsic conductivities, without external oxidative doping. These polymers show a technological interest due to their comparatively high thermal stabil-

Correspondence to: F. Mendizabal; e-mail: hagua@abello.dic.uchile.cl.

Contract grant sponsor: FONDECYT.
Contract grant number: 1990038.

ity and good semiconducting properties [29–31]. The experimental band gap values varied between 0.1 and 1.5 eV, which define them as semiconductors [32–36]. One of the factors responsible for the electrical conductivity in these complexes is the band gap, which may be approximated as the energy difference between the lowest unoccupied molecular orbital (LUMO) and highest occupied molecular orbital (HOMO) states.

The attention has been directed on bridged systems that contains central transition metal atoms, e.g., Co, Rh, Fe, etc. in the oxidation state +III. An appropriate bridging ligand may be a charged molecule such as cyanide (CN^-), which can generate the M′[MacM$(CN)_2$] complexes and [MacM$(CN)]_n$ polymers (M′ = Na, K; Mac = Pc, TBP; M = Co, Rh, Fe, Mn, Cr) [37–44]. All the cyano-bridged macrocycle metal complexes show comparatively high powder conductivities. For instance, the $[PcCoCN]_n$ polymer has a conductivity of 2×10^{-2} S/cm, with a band gap of about 0.10 eV [45, 46].

Theoretical studies of –[MacFe(L)$]_n$, with L = $C_2{}^{-2}$, CN^-, where Mac is a reduced macrocycle as tetraazaporphyrin (TAP), have been performed by using the tight-binding method based upon the extended Hückel formalism [47]. In that work, a semiconducting behavior of the systems like –[TAPFe(CN)$]_n$ was predicted. The band gap is mostly determined by the difference in energies between the LUMO of the macrocycle and the HOMO of the metal, this last state being formed by a mixture between transition metal d_{xz} and d_{yz} orbitals and π^* orbital of bridged ligand. However, the use of some reduced models to describe properties of semiconduction for real systems may be somehow different, as it has been previously demonstrated [48, 49]. Furthermore, since an intrinsic semiconductor is characterized by a small band gap and a lower density of highly mobile intrinsic charge carriers, it is necessary to use a more realistic model like the phthalocyaninato dianion.

In this work, the electronic structure of a series of [MacM$(CN)_2]^-$ complexes and [MacM$(CN)]_n$ polymers (Mac = Pc, TBP; M = Co, Rh) are investigated in detail through the density functional approach. We try to answer some questions concerning the electronic properties of the systems, such as: (i) What is the nature of the binding metal–cyanide? (ii) What is the nature and the magnitude of the band gap HOMO–LUMO? (iii) What is the relationship between the structural and electronic features of bridged ligands and their semiconducting properties? The study of the electronic structure of this family of compounds may help to rationalize the effects of several factors in the conducting properties of these materials.

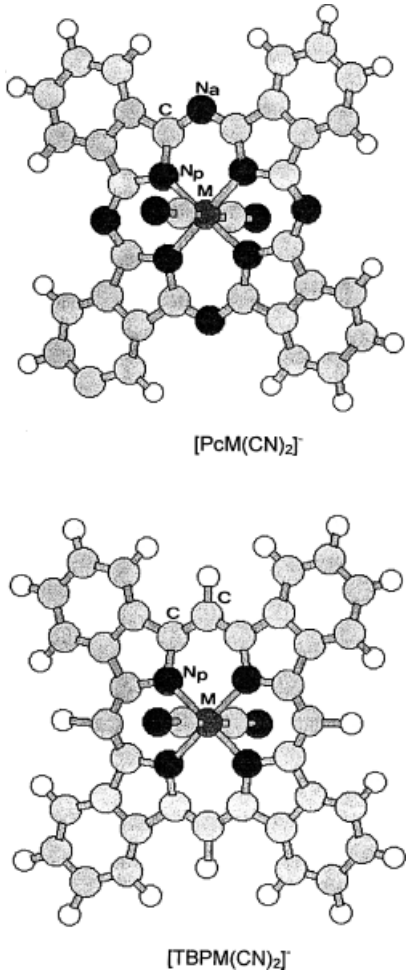

FIGURE 1. Structures of the metallomacrocycles $[PcM(CN)_2]^-$ and $[TBPM(CN)_2]^-$ (M = Co, Rh).

To answer these and other questions, we study the electronic structure of the complexes and the polymers as cyanide ligand, respectively (see Figs. 1 and 2).

Computational Details and Geometrical Parameters

The Amsterdam Density Functional [50, 51] (ADF 2.3 version) program package, based in the LCAO density functional for the complexes and polymers (ADF-band 1.0 version) [52] was used. Bonding energies were evaluated by the generalized transition-state method. We have included Becke's nonlocal

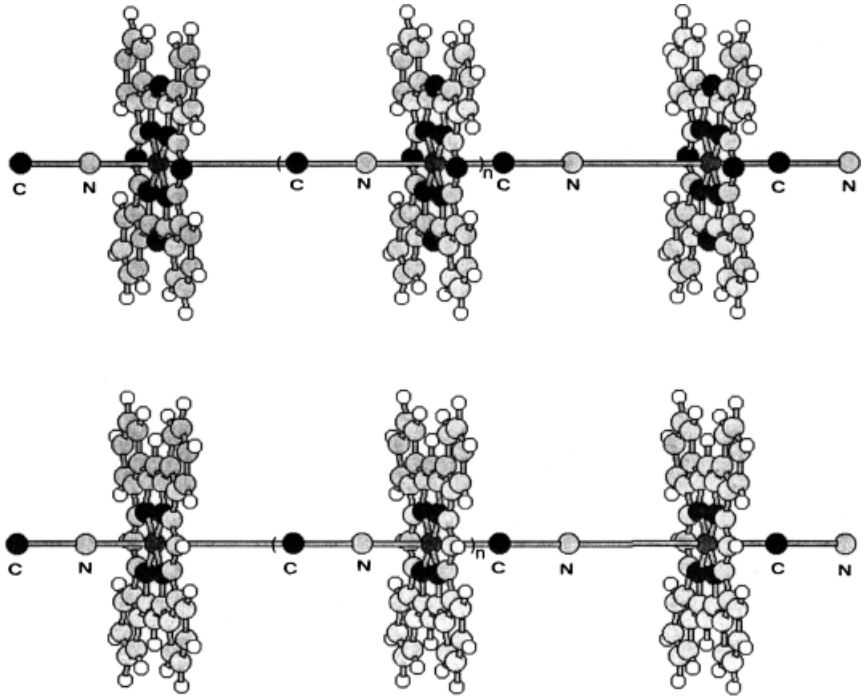

FIGURE 2. Structures of the metallomacrocycle polymers $[PcM(CN)]_n$ and $[TBPM(CN)]_n$ (M = Co, Rh).

correction [53] to the local HFS exchange energy [local density approximation (LDA)] was well as Stoll's correction [54] for correlation between electrons of different spins, based on Vosko et al. [55] parametrization from electron gas data. This Hamiltonian has demostrated to give an excellent description of systems with metallomacrocycles [56–58].

Moreover, to perform the calculation on the polymers, we have used the ADF band code at the LDA level of theory and nonlocal gradient corrections by Becke for the exchange energy. All the calculations were performed with an integration accuracy greater than 10^{-4} and at 10 k points in the reduced Brillouin zone for all the one-dimensional (1D) cells.

The molecular orbitals were expanded in an uncontracted double-ξ Slater-type orbital (STO) basis set [59] for all atoms with the exception of the transition metal (Co, Rh) orbitals, for which we used a triple-ξ basis set. One 4p and 5p STO polarization functions were used for Co and Rh, respectively. The cores (Co: 1s-2p; Rh: 1s-3p; C, N: 1s) were kept frozen [50, 51]. For the polymers, we used a basis set of numerical atomic orbital (NAOs) obtained from the STOs for each atom.

We are interested in estimating the band gap of these systems. In the context of density functional theory (DFT) the energy gap is twice the hardness η [60, 61]. This last quantity is defined as [62]

$$\eta = \frac{1}{2}\left(\frac{\partial^2 E}{\partial N^2}\right)_{\nu} \cong \frac{I - A}{2}, \tag{1}$$

where E is the electronic energy, N is the number of electrons, ν is the external potential, I is the ionization potential, and A is the electron affinity. Working definitions of the quantities I and A are possible within molecular theory [63, 64]. According to Koopmans's theorem, the ionization potential and electron affinity may be approximated in the molecular orbital theory as $I \cong -\varepsilon_{\mathrm{HOMO}}$ and $A \cong -\varepsilon_{\mathrm{LUMO}}$ [65], respectively. With these approximations, the hardness is just half the energy gap between highest occupied molecular orbital (HOMO) and lowest unoccupied molecular orbital (LUMO):

$$\eta \cong \frac{\varepsilon_{\mathrm{LUMO}} - \varepsilon_{\mathrm{HOMO}}}{2}. \tag{2}$$

A bigger η means a large I and a smaller A, which implies that the system has a smaller tendency to accept electrons and/or a smaller tendency to give away electrons. Thus, hardness can be seen as a resistance to charge transfer [66]. For solids, η is the half of the energy gap (ΔE_{gap}) [66]:

$$\eta = \frac{\Delta E_{\mathrm{gap}}}{2}. \tag{3}$$

The conductivity (σ) of a semiconductor depends on the energy required to promote electrons from the Fermi level across the band gap (E_g) [67, 68]. Therefore, we qualitatively associate the magnitude of η and energy gap with the property of semiconductivity in the systems under study [64]. Thus, we will have an approximated index to compare and to explain the experimental values as conductivity and band gap.

We have first performed calculations on the isolated MacM [M = Co, Rh; Mac = phthalocyanine (Pc), tetrabenzoporphyrine (TBP)] molecules using the experimental geometry (X-ray data) [37–41], with appropriate averaging of bond angles and bond lengths to maintain the D_{4h} symmetry. The monomers have been built up by linking MacM (metallomacrocycle) with CN^-, metal over ligand, along the stacking direction (z axis in our coordinate system). Figure 1 shows the molecular stacking. The bridged structure shown in Figure 2 has been confirmed for many compounds using a variety of physical methods [infrared (IR), Mössbauer spectroscopy, nuclear magnetic resonance (NMR), thermogravimetry, and scanning tunneling microscopy] [37–46]. The crystal structure of $K[PcCo(CN)_2]$ is known and confirms the bisaxial coordination of the CN^- groups. Powder X-ray diffraction measurements give evidence about an isostructural lattice in the compounds $[PcM(CN)]_n$ (M = Cr, Mn, Fe, Co, Rh).

The geometry of the $[PcCo(CN)_2]^-$ moiety is experimentally known. For the remaining complexes ($[PcRh(CN)_2]^-$, $[TBPCo(CN)_2]^-$, $[TBPRh(CN)_2]^-$), this information is not available. Therefore, we perform a partial optimization of the metal–CN and the C≡N distances, and the remaining part of the structure of the complexes is kept frozen at the experimental geometry of the respective monomers.

Results and Discussion

$[MacM(CN)_2]^-$ COMPLEXES (Mac = Pc, TBP; M = Co, Rh)

We performed a fragmentation analysis on $[MacM(CN)]_n$ polymers from their respective monomers. Building up these models stepwise, the molecular approach should depict the frontier orbitals implicated in the valence (highest occupied) and conduction (lowest unoccupied) bands. We analyzed the electronic structure of the $[MacM(CN)_2]^-$ complexes (Mac = Pc, TBP; M = Co, Rh) through fragments in which the $(CN)_2{}^{-2}$ unit interacts with the [MacM] metallomacrocycle.

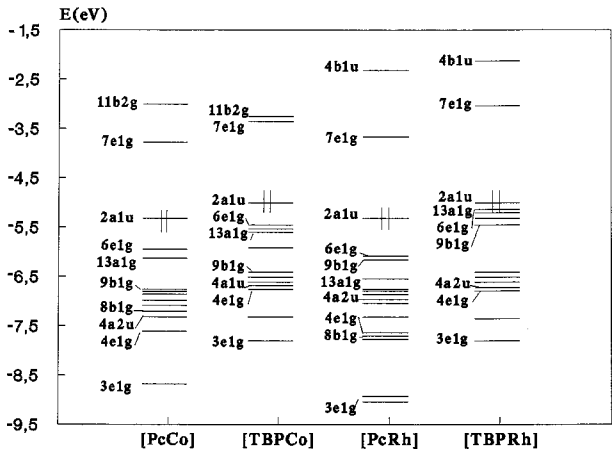

FIGURE 3. Energy level scheme for PcCo, TBPCo, PcRh, and TBPRh. Double occupancy is indicated for the HOMO. All lower-lying orbitals are also double occupied, except for $13a_{1g}$ (singly occupied).

The [MacM] fragment has D_{4h} geometry. Figure 3 shows the one-electron levels obtained by restricted calculations for the metallomacrocycles series. The ground states of MacM complexes are $^2A_{1g}$, with occupation of the one-electron levels as indicated in Figure 3. It is clear that the highest fully occupied molecular orbital is invariably the $2a_{1u}$ level, which is a pure macrocycle orbital and lies in all the systems, within the same range of energy. This theoretical result confirms the experimental evidence based on the electrochemical behavior obtained by cyclic voltammetry of compounds $A[MacM(CN)_2]$ (A = Na, K; Mac = Pc, TBP; M = Co, Rh, Fe, Ru, Cr, Mn). Therein, it was demonstrated that the first oxidation process occurs on the macrocycle ring [69].

For a discussion of the trends in the one-electron energies, it is instructive to look at the composition of the individual orbitals. In Table I, the composition of the most important orbitals is given in terms of metal and macrocycle contributions. Our results indicated an increasing energy level order of the metal orbitals, $d_{x^2-y^2} > d\pi(d_{xz}, d_{yz}) > d_{z^2} > d_{xy}$, which are in agreement with previously reported calculations [56–58]. We assumed an electronic ground-state configuration of metal $(d\pi)^3(d_{z^2})^1(d_{xy})^2$. The LUMO orbital, $7e_g(\pi^*)$, emerges by an interaction between the $d\pi$ orbital of metal and the $6e_g(\pi^*)$ orbital of the Mac^{-2}.

The metallotetrabenzoporphyrine complexes show a similar molecular orbital diagram to that

TABLE I

Percent contribution of macrocycle (Mac) and metal (M) fragments to selected orbitals (based on Mulliken population analysis per MO) of metallomacrocycle, where only the main contributions to each orbital have been given.

		ε (eV)	M	Mac
$7e_{1g}$	PcCo	−3.762	4.70 (d_x)	95.3 (p_z)
	TBPCo	−3.278	3.50 (d_x)	96.5 (p_z)
	PcRh	−3.668	6.00 (d_x)	94.0 (p_z)
	TBPRh	−3.017	15.1 (d_x)	84.9 (p_z)
$11b_{2g}$	PcCo	−2.933	61.6 (d_{xy})	38.2 (N_p lone pair)
	TBPCo	−3.267	64.6 (d_{xy})	35.4 (N_p lone pair)
$4b_{1u}$	PcRh	−2.293	0.00	100 (on the ring)
	TBPRh	−2.110	0.00	100 (on the ring)
$2a_{1u}$	PcCo	−5.345	0.00	100 ($2a_{1u}$ from Pc^{-2})
	TBPCo	−5.009	0.00	100 ($2a_{1u}$ from TBP^{-2})
	PcRh	−5.335	0.00	100 ($2a_{1u}$ from Pc^{-2})
	TBPRh	−5.029	0.00	100 ($2a_{1u}$ from TBP^{-2})
$6e_{1g}$	PcCo	−5.980	61.5 (d_π)	38.5 (p_z)
	TBPCo	−5.455	68.9 (d_π)	31.1 (p_z)
	PcRh	−6.081	37.8 (d_π)	62.2 (p_z)
	TBPRh	−5.120	62.3 (d_π)	37.7 (p_z)
$13a_{1g}$	PcCo	−6.117	96.6 (d_{z^2}, 4s)	3.40
	TBPCo	−5.483	97.5 (d_{z^2}, 4s)	2.50
	PcRh	−6.542	89.7 (d_{z^2}, 5s)	10.3
	TBPRh	−5.215	95.3 (d_{z^2}, 5s)	4.70
$9b_{1g}$	PcCo	−6.142	48.4 ($d_{x^2-y^2}$)	51 .6 (N_a lone pair)
	TBPCo	−5.925	96.1 ($d_{x^2-y^2}$)	3.90 (C_a lone pair)
	PcRh	−6.180	26.9 ($d_{x^2-y^2}$)	73.1 (N_a and N_p)
	TBPRh	−5.344	92.3 ($d_{x^2-y^2}$)	7.70 (C_a lone pair)
$8b_{1g}$	PcCo	−7.081	48.3 ($d_{x^2-y^2}$)	51.7 (N_a lone pair)
	PcRh	−7.722	64.7 ($d_{x^2-y^2}$)	35.3 (N_a lone pair)
$4a_{2u}$	PcCo	−7.197	2.90 (p_z)	97.1 ($4a_{2u}$)
	TBPCo	−6.591	0.80 (p_z)	99.2 ($4a_{2u}$)
	PcRh	−7.302	2.90 (p_z)	97.2 ($4a_{2u}$)
	TBPRh	−6.590	0.40 (p_z)	99.6 ($4a_{2u}$)
$4e_{1g}$	PcCo	−7.314	23.9 (d_π)	76.1 (p_z)
	TBPCo	−6.715	20.6 (d_π)	78.7 (p_z)
	PcRh	−7.692	27.8 (d_π)	72.2 (p_z)
	TBPRh	−6.744	12.7 (d_π)	87.3 (p_z)
$3e_{1g}$	PcCo	−8.722	5.80 (d_π)	94.2 (p_z)
	TBPCo	−7.786	1.30 (d_π)	98.7 (p_z)
	PcRh	−9.032	16.0 (d_π)	84.0 (p_z)
	TBPRh	−7.803	1.30 (d_π)	98.7 (p_z)

of PcM. However, there are slight but important differences in the location on the energy levels. The nitrogen atoms in the aza positions of the [PcM] were replaced by –CH groups. Due to the lower electronegativity of the –CH groups, they produce a smaller stabilization of the antibonding π^* system in the macrocycle, and therefore a great HOMO–LUMO gap. This is agreement with the second-or-

der perturbation theory at the electronegativity level [70].

The fragmentation analysis was performed in order to know what happens when the metallomacrocycle [MacM] is connected with the cyano-bridged ligand. The introduction of an axial ligand CN^- modifies the ground-state electronic configuration of metallomacrocycles described in the previous section. Experimental evidence confirm that the central metal atom shows an oxidation state +III in $[MacM(CN)_2]^-$ complexes, as well as $[MacMCN]_n$ polymers [37–41]. These compounds show an electron spin resonance (ESR) silent sign, associated to a restricted electronic state [45, 46].

We start analyzing the frontier orbitals of $[MacM(CN)_2]^-$ (Mac = Pc, TBP; M = Co, Rh) monomers. Figure 4 shows the principal orbital interactions between these two fragments: $[MacCo(III)]^+$ and $(NC{-}{-}{-}CN)^{-2}$. For both fragments, the electronic levels have been rigidly shifted to lower energies in order to bring the $2a_{1u}$ level as a reference to evaluate the perturbation effects when the complex is formed. As expected, the d_{z2} orbital is highly destabilized by the σ interactions with the $3a_{1g}$ orbital of the CN^- ligands. Furthermore, the destabilization promoted by the π donation of the $d(\pi)$ orbitals ($6e_{1g}$) to $2e_{1g}$ of the CN^- ligands appears to be strong enough to increase the back-bonding from the metal to the bridged ligands, which has a higher contribution from the macrocycle ring. For the complexes studied, an atomic orbital population analysis is given in Table II for some selected molecular orbitals.

As mentioned before, our main interests in this work is to focus on the electronic properties. Therefore, we analyzed the HOMOs and LUMOs. In the monomers, the HOMO and LUMO are the same frontier orbitals of MacM, which do not change upon formation of the complexes. Moreover, these orbitals are practically fixed in energy for the set of monomers. The HOMO ($2a_{1u}$) is a pure macrocycle orbital, while the LUMO ($8e_{1g}$) is composed of the LUMOs of the Mac ring and a small contribution of the $d\pi$ orbital of the metal. We have included the composition of the virtual orbital $16a_{1g}$, since when the polymers are formed such orbital have an important role. This orbital is σ antibonding, with the composition d_{z2} (~52%) on the metal center, and $2p_z$ for C and N (~35%).

We have accomplished an analogous analysis for the complexes of rhodium (see Fig. 5). The results for such systems are very similar to those for cobalt.

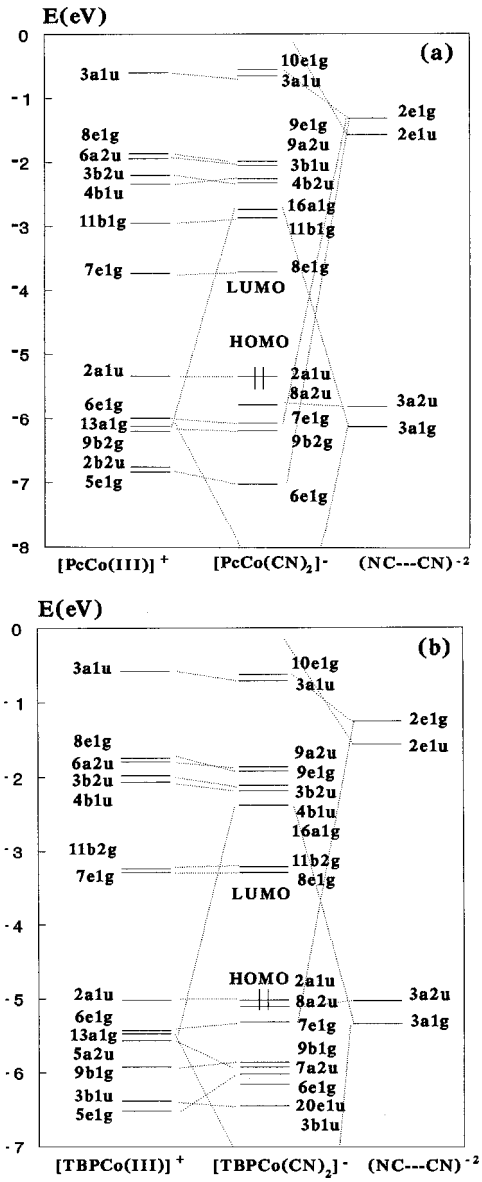

FIGURE 4. Interaction diagrams of $[MacCo(CN)_2]^-$. (a) Mac = Pc^{-2}. (b) Mac = TBP^{-2}. On the side and right side are the levels of $[MacCo(III)]^+$ and $(NC{-}{-}{-}CN)^{-2}$, respectively.

We have calculated the hardness values of the complexes studied from Eq. (2). The results are summarized in Table III. The smaller the hardness value, the better will be the semiconduction. Furthermore, it can be seen that when the number of nitrogen atoms in the macrocycle increases (from TBP to Pc), the semiconduction is enhanced. This may be traced to the higher electronegativity of nitrogen compared to that of the –CH group, thereby producing a greater stabilization of the macrocycle's

TABLE II

Percentage contribution of individual fragments to selected orbitals (based on Mulliken population analysis per MO) of $[MacM(CN)_2]^-$ with Mac = Pc, TBP; M = Co, Rh.

		ε (eV)	M	Mac	CN^-
$16a_{1g}$	$[PcCo(CN)_2]^-$	−2.704	52.9 (d_{z2}, 4s)	10.8 (p_z, on the ring)	36.3 (p_z)
	$[TBPCo(CN)_2]^-$	−2.372	52.3 (d_{z2}, 4s)	16.1 (p_z, on the ring)	31.6 (p_z)
	$[PcRh(CN)_2]^-$	−1.802	52.8 (d_{z2}, 4s)	9.36 (p_z, on the ring)	37.8 (p_z)
	$TBPRh(CN)_2]^-$	−1.495	53.5 (d_{z2}, 4s)	12.0 (p_z, on the ring)	34.5 (p_z)
$11b_{2g}$	$[PcCo(CN)_2]^-$	−2.862	60.4 (d_{xy})	39.6 (N_p lone pair)	0.00
	$[TBPCo(CN)_2]^-$	−3.213	63.4 (d_{xy})	36.6 (N_p lone pair)	0.00
$4b_{1u}$	$[PcRh(CN)_2]^-$	−2.382	0.00	100 (on the ring)	0.00
	$[TBPRh(CN)_2]^-$	−2.240	0.00	100 (on the ring)	0.00
$8e_{1g}$	$[PcCo(CN)_2]^-$	−3.698	4.30 (d_π)	95.7 (on the ring)	0.00
	$[TBPCo(CN)_2]^-$	−3.230	3.11 (d_π)	96.9 (on the ring)	0.00
	$[PcRh(CN)_2]^-$	−3.607	5.81 (d_π)	94.2 (on the ring)	0.00
	$[TBPRh(CN)_2]^-$	−3.197	4.69 (d_π)	95.3 (on the ring)	0.00
$2a_{1u}$	$[PcCo(CN)_2]^-$	−5.345	0.0	100 ($2a_{1u}$ from Pc^{-2})	0.00
	$[TBPCo(CN)_2]^-$	−5.009	0.0	100 ($2a_{1u}$ from TBP^{-2})	0.00
	$[PcRh(CN)_2]^-$	−5.335	0.0	100 ($2a_{1u}$ from Pc^{-2})	0.00
	$[TBPRh(CN)_2]^-$	−5.029	0.0	100 ($2a_{1u}$ from TBP^{-2})	0.00
$8a_{2u}$	$[PcCo(CN)_2]^-$	−5.758	6.11	44.4 (N_p, p_z)	49.5 (p_z)
	$[TBPCo(CN)_2]^-$	−5.245	6.63	37.5 (C, p_z)	55.9 (p_z)
	$[PcRh(CN)_2]^-$	−5.947	5.59	35.0 (N_p, p_z)	59.4 (p_z)
	$[TBPRh(CN)_2]^-$	−5.180	4.91	73.1 (C, N_p, p_z)	22.0 (p_z)
$7e_{1g}$	$[PcCo(CN)_2]^-$	−5.860	59.8 (d_π)	18.6 (p_z)	21.6 (p_y)
	$[TBPCo(CN)_2]^-$	−5.304	63.1 (d_π)	6.78 (p_z)	30.1 (p_y)
	$[PcRh(CN)_2]^-$	−5.958	40.5 (d_π)	39.2 (p_z)	20.3 (p_y)
	$[TBPRh(CN)_2]^-$	−5.431	45.5 (d_π)	30.3 (p_z)	24.2 (p_y)
$9b_{1g}$	$[PcCo(CN)_2]^-$	−6.087	48.2 ($d_{x^2-y^2}$)	51.8 (N_a lone pair)	0.00
	$[TBPCo(CN)_2]^-$	−5.876	96.3 ($d_{x^2-y^2}$)	3.70 (C_a lone pair)	0.00
	$[PcRh(CN)_2]^-$	−6.117	47.9 ($d_{x^2-y^2}$)	52.1 (N_a and N_p)	0.00
	$[TBPRh(CN)_2]^-$	−6.334	90.5 ($d_{x^2-y^2}$)	9.49 (C_a lone pair)	0.00
$6e_{1g}$	$[PcCo(CN)_2]^-$	−6.545	0.00	41.9 (p_z)	58.1 (p_y)
	$[TBPCo(CN)_2]^-$	−6.036	0.00	30.7 (p_z)	69.3 (p_y)
	$[PcRh(CN)_2]^-$	−6.117	0.00	31.7 (p_z)	68.3 (p_y)
	$[TBPRh(CN)_2]^-$	−6.170	0.00	66.4 (p_z)	33.6 (p_y)
$15a_{1g}$	$[PcCo(CN)_2]^-$	−7.094	13.9 (d_{x^2}, 4s)	2.16	83.9 (σ)
	$[TBPCo(CN)_2]^-$	−6.628	13.9 (d_{x^2}, 4s)	1.78	84.3 (σ)
	$[PcRh(CN)_2]^-$	−7.215	9.19 (d_{x^2}, 5s)	3.56	87.3 (σ)
	$[TBPRh(CN)_2]^-$	−6.653	9.77 (d_{x^2}, 5s)	3.22	87.0 (σ)

LUMO, and therefore a reduction in the HOMO–LUMO gap [70].

$[MacM(CN)]_n$ POLYMERS

When going from the complex to the infinite chain, due to the stacked effects of MacM units, we would expect a smaller energy gap. Table IV shows such an effect for the systems with PcM (M = Co, Rh) in monomers and polymers, respectively. The gap is reduced upon formation of the polymer.

We have described the frontier band structures for the $[MacM(CN)]_n$ polymers with Mac = Pc, TBP; M = Co, Rh. Only the highest occupied crys-

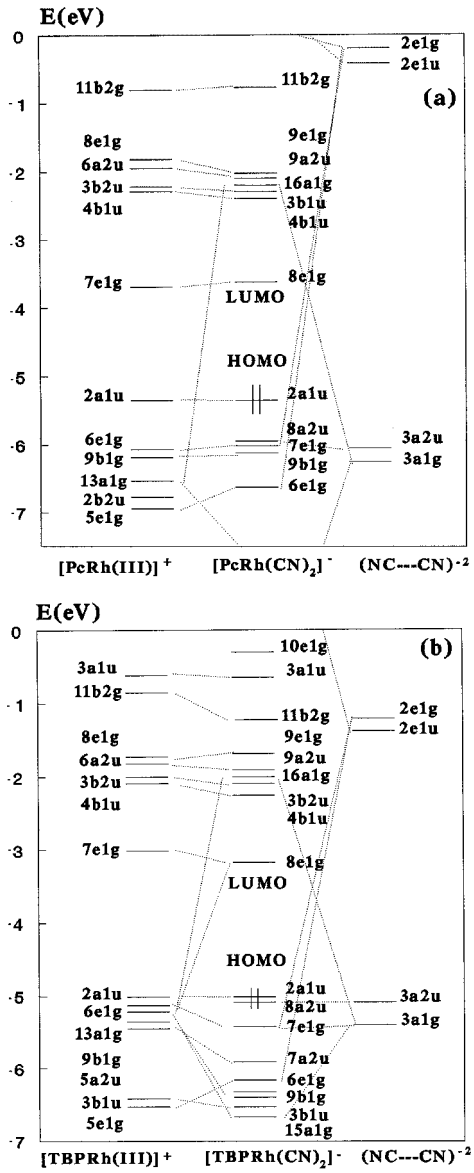

FIGURE 5. Interaction diagrams of $[MacRh(CN)_2]^-$. (a) Mac = Pc^{-2}. (b) Mac = TBP^{-2}. On the side and right side are the levels of $[MacRh(III)]^+$ and $(NC{-}{-}{-}CN)^{-2}$, respectively.

tal orbitals (HOCOs) and the lowest unoccupied CO (LUCOs) are shown in the range −6.5 to −1.5 eV in Figures 6 and 7. There are several flat bands that correspond to well-localized electrons. The bands for these systems can be classified according to the D_{4h} group at the edges and center of the Brillouin zone but only according to the C_{4v} group at all other points in the k space. Among them, we found that the bands fall within the −5.0- to −6.5-eV range, which is associated to the HOCO corresponding to

TABLE III
Hardness results for $[MacM(CN)_2]^-$ complexes.[a]

Complex	LUMO	HOMO	η
$[PcCo(CN)_2]^-$	−3.698	−5.345	0.824
$[TBPCo(CN)_2]^-$	−3.230	−4.894	0.832
$[PcRh(CN)_2]^-$	−3.607	−5.335	0.864
$[TBPRh(CN)_2]^-$	−3.197	−5.029	0.916

[a] Energies in eV.

a_2 ($2a_{1u}$ in complex), a_1 ($8a_{2u}$), e (as the π bands), and b_2 (d_{xy}) of the Co atom in both Pc and TBP (see Fig. 6). The same behavior was found for the rhodium compounds (see Fig. 7).

On the other hand, when we center our attention on the conduction band (LUCO), a different situation is appreciated. The Bloch functions at the center ($k = 0, \Gamma$) and edge ($k = \pi/a, Z$) of the Brillouin zone were used. First, we analyze the $[MacCo(CN)]_n$ polymers. The LUCO band for the polymers runs down toward the Z vector, which in turn corresponds to the most bonding combination. This band shows a_1 symmetry, which is associated with the $16a_{1g}$ orbital of the complexes of cobalt (LUMO+2). This band shows a σ interaction between the linear chain of atoms. The band structure derived from the σ orbitals is given in Figure 8. There is also a small contribution of a pair of e_g macrocycle (Pc and TBP) orbitals not shown for simplicity. The net result is a band that is antibonding for Γ ($k = 0$) and bonding for Z ($k = \pi/a$).

When we analyze the polymers with rhodium, $[MacRh(CN)]_n$, the band structures show a similar

TABLE IV
Summary of results[a] for (i) $[PcCo(CN)]_n$, (ii) $-[PcRh(CN)]_n$, (iii) $[PcCo(CN)_2]^-$, and (iv) $[PcRh(CN)_2]^-$.

	i[b]	ii[b]	iii	iv
HOMO[c]	−5.361	−5.345	−5.345	−5.335
LUMO[d]	−4.083	−3.967	−3.698	−3.607
Energy gap[e]	1.278	1.378	1.647	1.728

[a] Energy in eV.
[b] For polymers (i) and (ii), the corresponding terms are HOCO, LUCO.
[c] Highest occupied molecular orbital.
[d] Lowest unoccupied molecular orbital.
[e] Transition energy between the HOMO and the LUMO.

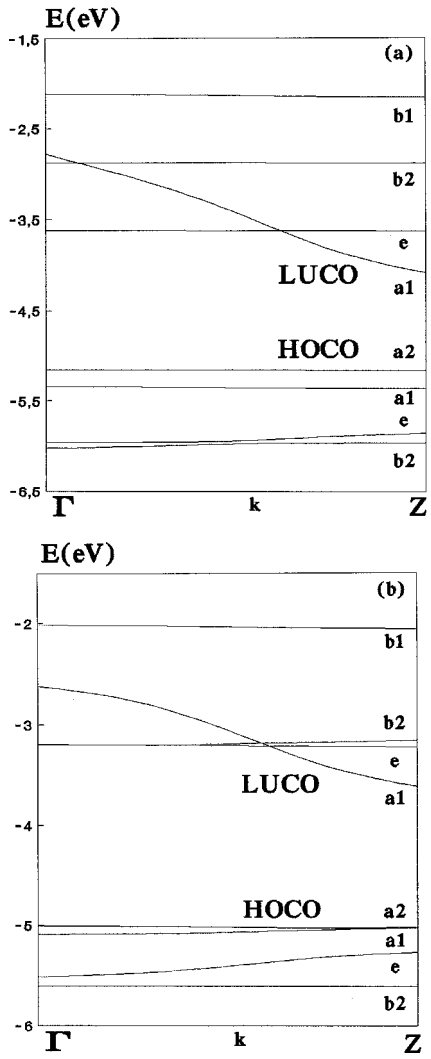

FIGURE 6. Band structures for (a) $[PcCo(CN)]_n$ and (b) $[TBPCo(CN)]_n$.

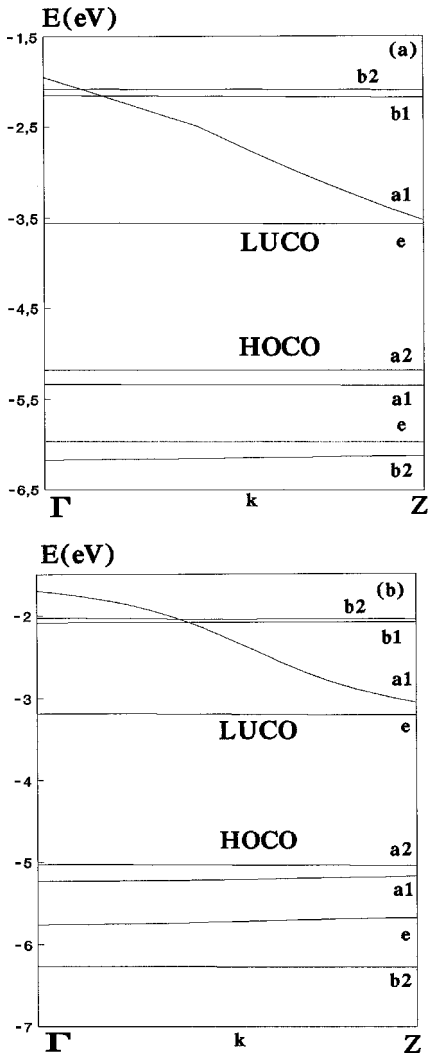

FIGURE 7. Band structures for (a) $[PcRh(CN)]_n$ and (b) $[TBPRh(CN)]_n$.

diagram such as that previously analyzed for cobalt. However, there are slight but important differences in the location on the a_1 band (see Fig. 7). For these polymers of the a_1 band, with composition similar to that of cobalt polymers, the atoms have less σ interactions. Then, this band cannot be stabilized beyond the e band (with a composition between $d\pi$ orbitals of metal and π^* orbitals of the Mac). This last represents the band LUCO of these polymers.

We have also built up the density of states (DOS) [71, 72] and its projection on the metal and cyano-bridged ligand for the $[PcM(CN)]_n$ (M = Co, Rh) polymers (Fig. 9). For both polymers, the valence band (VB) shows the same composition: It is centered in the ring. On the other hand, the conduction band (CB) shows a composition that depends on the polymer: For the system with cobalt, the projections of the metal and bridged ligand orbitals in the density of states showed a mixture of both com-

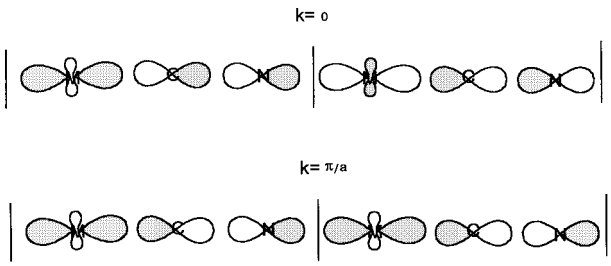

FIGURE 8. Sketch of the orbital composition of a_1 band virtual for $[MacM(CN)]_n$.

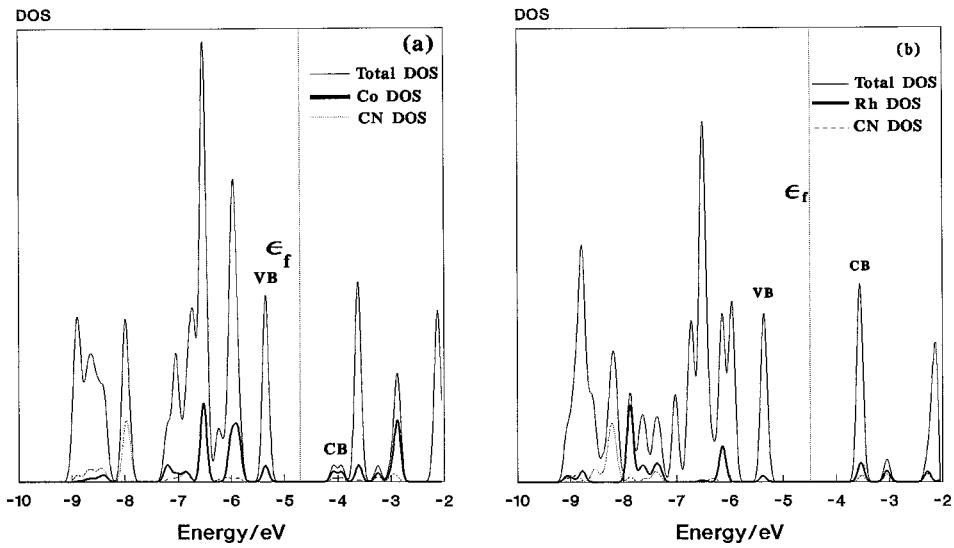

FIGURE 9. Density of states for $[PcM(CN)]_n$ polymers with the projections metal (M) and cyanide (CN^-) which illustrate the nature of the frontier crystal orbital: (a) $[PcCo(CN)]_n$ and (b) $[PcRh(CN)]_n$.

ponents. When the polymer has rhodium, the CB is centered on the ring.

We have summarized the results for the polymers studied including experimental measurements (conductivity and energy band gap) [37–47] in Table V. The metallomacrocycle polymers with cyano-bridged ligand showed semiconducting properties, with a similar tendency as the experimental measurements of conductivity and band gap. However, the theoretical results are overestimated with respect to the experimental in an order of magnitude. This trend is opposite to the results in solid state for different approximate density functionals, since the energy band gap is underestimated by 20–50% [73, 74].

We believe that such differences should be traced to the use of Eq. (2). This formula is applied commonly in Hartree–Fock theory, but here we are using the Kohn–Sham scheme. In spite of this, we have been able to reproduce the experimental trend, therefore Eq. (2) provides only a qualitative relationship.

Conclusions

The analysis of the electronic structures of the polymers and complexes indicate that (i) the HOCO is very flat band, largely composed of the macrocycle orbitals, and (ii) the LUCO band is composed by a mixture between the cobalt and cyanide bridged

TABLE V
Summary of computational results[a] for the –[MacM(CN)]$_n$ polymers.[b]

Polymer	LUCO[c]	HOCO[d]	Energy gap theoretical[e]	Band gap experimental	σ
$[PcCo(CN)]_n$	−4.083	−5.361	1.278	0.10	2×10^{-2}
$[TBPCo(CN)]_n$	−3.618	−5.024	1.406	0.11	4×10^{-2}
$[PcRh(CN)]_n$	−3.566	−5.345	1.738		4×10^{-4}
$[TBPRh(CN)]_n$	−3.204	−5.029	1.824		

[a] Energy in eV.
[b] Experimental energy gaps and conductivity (σ, S/cm) [8, 10].
[c] Lowest unoccupied crystal orbital.
[d] Highest occupied crystal orbital.
[e] Transition energy between the HOCO and the LUCO.

ligand orbitals, for the case of the systems formed by Pc and TBP. This composition is completely different when the metal is rhodium. Such a band is exclusively composed of the π^* system of macrocycle, but a band very close to it shows a strong composition of Rh and CN^- groups. It is interesting to note that our predicted conductivities fall in the same range as the experimental conductivity.

ACKNOWLEDGMENTS

This work was supported by FONDECYT project no. 1990038. Also, the author thanks Dr. Luis Padilla (Comisión Chilena de Energía Nuclear) for access to the ADF 2.3 version package.

References

1. Kellog, G. E.; Gaudiello, J. G. In Bruce, D. W.; O'Hare, D., Eds. Polymeric Coordination Complexes: Bridging Molecular Metals and Conductive Polymers. Inorganic Materials; Wiley: New York, 1992; pp. 353–404.
2. Zeldin, M.; Wynne, K. J.; Allcock, H. R. In Inorganic and Organometallic Polymers; ACS Symposium Series; 1988, Vol. 360.
3. Cassoux, P.; Valade, L. In Bruce, D. W.; O'Hare, D., Eds. Molecular Inorganic Superconductors, Inorganic Materials; Wiley: New York, 1992; pp. 1–58.
4. Rosenblum, M. Adv Mater 1996, 6, 159.
5. Böhm, M. C. In One-Dimensional Organometallic Materials; Lectures Notes in Chemistry, No. 4; Springer: 1988.
6. Deger, S.; Lange, A.; Hanack, M. Chem Coord Rev 1988, 83, 115.
7. Marks, T. Science 1995, 227, 881.
8. Schultz, H.; Lehmann, H.; Rein, M.; Hanack, M. Struct Bonding 1991, 74, 41.
9. Hanack, M. Macromol Symp 1994, 80, 83.
10. Hanack, M.; Lang, M. Adv Mater 1994, 6, 819.
11. Hanack, M. GIT Fachz Lab 1987, 2, 75.
12. Fernandez, F.; Torres, T.; Hauschel, B.; Hanack, M. Chem Rev 1998, 98, 563.
13. Bryce, M. R. Chem Br 1988, 781.
14. Chen, C.-T.; Suslick, K. S. Coord Chem Rev 1993, 128, 193.
15. Hanack, M.; Knecht, S.; Schulte, M. J Organometallic Chem 1993, 445, 157.
16. Knecht, S.; Polley, R. Chem Ber 1995, 128, 928.
17. Pohmer, J.; Hanack, M.; Barcina, J. J Mater Chem 1996, 6, 957.
18. Kang, Y. G.; Kim, H. Synth Met 1997, 78, 11.
19. Hanack, M.; Lange, A.; Grosshans, R. Synth Met 1991, 45, 59.
20. Kleinwachter, J.; Hanack, M. J Am Chem Soc 1997, 119, 10684.
21. Hanack, M.; Fischer, K. Synth Met 1985, 10, 345.
22. Ziener, U.; Fahmy, N.; Hanack, M. Chem Ber 1996, 126, 2559.
23. Bulatov, A.; Knecht, S.; Subramanian, L. R. Chem Ber 1993, 126, 2565.
24. Hanack, M.; Polley, R. Inorg Chem 1994, 33, 3201.
25. Collman, J. P.; McDevitt, J. T.; Leidner, C. R. J Am Chem Soc 1987, 109, 4606.
26. Hiller, R.; Hanack, M.; Mezgar, M. Acta Cryst C 1987, 43, 1264.
27. Hanack, M.; Gül, A.; Subramanian, L. R. Inorg Chem 1992, 31, 1542.
28. Keppler, U.; Deger, S.; Lange, A.; Hanack, M. Angew Chem Int Ed Engl 1987, 26, 724.
29. Meier, H.; Albrecht, W.; Zimmerhackl, E.; Hanack, M.; Metz, J. J Synth Met 1985, 11, 333.
30. Meier, H.; Albrecht, W.; Hanack, M.; Koch, J. Polymer Bull 1986, 16, 75.
31. van Nostrum, C. F.; Nolte, R. J. Chem Commun 1996, 2385.
32. Diel, B. N.; Inabe, T.; Jaggi, N. K.; Lyding, J. W.; Schneider, O.; Hanack, M.; Kannewurf, C. R.; Marks, T. J.; Schwartz, L. H. J Am Chem Soc 1984, 106, 3207.
33. Kleinwächter, J.; Hanack, M. J Am Chem Soc 1997, 119, 10684.
34. Gaudillo, J. G.; Kellogg, G. E.; Tetrick, S. M.; Marks, T. J. J Am Chem Soc 1989, 111, 5259.
35. Hanack, M.; Schlick, U. Inorg Chem 1995, 34, 3621.
36. Schneider, O.; Hanack, M. Chem Ber 1983, 116, 2088.
37. Inable, T.; Maruyama, Y. Chem Lett 1989, 55.
38. Inable, T.; Maruyama, Y. Bull Chem Soc Jpn 1990, 63, 2273.
39. Datz, A.; Metz, J.; Schneider, O.; Hanack, M. Synth Met 1984, 9, 31.
40. Münz, X.; Hanack, M. Chem Ber 1988, 121, 239.
41. Williams G. A.; Figgis, B. N. J Chem Soc 1980, 1688.
42. Hanack, M.; Polley, R.; Knecht, S.; Schlick, U. Inorg Chem 1995, 34, 3621.
43. Hanack, M.; Hedtmann-Rein, C. Z Naturforsch 1985, 40b, 1087.
44. Ziener, U.; Fahmy, N.; Hanack, M. Chem Ber 1993, 126, 2559.
45. Metz, J.; Hanack, M. J Am Chem Soc 1983, 105, 828.
46. Hanack, M.; Hedtmann-Rein, C.; Datz, A.; Keppeler, U.; Münz, X. Synth Met 1987, 19, 787.
47. Canadell, E.; Alvarez, S. Inorg Chem 1984, 23, 573.
48. Mendizabal, F.; Olea-Azar, C.; Zapata-Torres, G.; Eisner, F. Theochem, to appear.
49. Mendizabal, F.; Olea-Azar, C.; Briones, R. Int J Quantum Chem 2001, 82, 170.
50. Baerends, E. J.; Ellis, D. E.; Ros, P. Chem Phys 1973, 2, 42.
51. Baerends, E. J.; Ros, P. Int J Quantum Chem 1978, S12, 169.
52. te Velde, G.; Baerends, E. J. Phys Rev B 1991, 44, 7888.
53. Becke, A. D. J Chem Phys 1986, 84, 4524.
54. Stoll, H.; Golka, E.; Preuss, E. Theor Chim Acta 1980, 29, 55.
55. Vosko, S. H.; Wilk, L.; Nusair, M. J Can J Phys 1980, 58, 1200.
56. Rosa, A.; Baerends, E. J. Inorg Chem 1992, 31, 4717.
57. Rosa, A.; Baerends, E. J. Inorg Chem 1993, 32, 5637.
58. Rosa, A.; Baerends, E. J. Inorg Chem 1994, 33, 584.
59. Snijders, J. G.; Vernooijs, P.; Baerends, E. J. At Data Nucl Data Tables 1982, 26, 483.
60. Parr, R. G.; Yang, W. In Density Functional Theory of Atoms and Molecules; Oxford University Press: New York, 1989.

61. Kohn, W.; Becke, A. D.; Parr, R. G. J Phys Chem 1996, 100, 12974.
62. Parr, R. G.; Pearson, R. G. J Am Chem Soc 1983, 105, 7512.
63. Pearson, R. G. Acc Chem Res 1993, 26, 250.
64. Person, R. G. In Chemical Hardness; Wiley-VCH: 1997.
65. Koopman, T. A. Physica 1933, 1, 104.
66. Parr, R. G.; Zhou, Z. Acc Chem Res 1993, 26, 256.
67. Mendizabal, F.; Contreras, R.; Aizman, A. Int J Quantum Chem 1995, 56, 820.
68. Mendizabal, F.; Contreras, R.; Aizman, A. J Phys Condens Matter 1997, 9, 30.11.
69. Behnisch, R.; Hanack, M. Synth Met 1990, 36, 387.
70. Albright, T. A.; Burdett, J. K.; Whangbo, M.-H. In Orbital Interactions in Chemistry; Wiley: New York, 1985.
71. Yu, H. L. Phys Rev B 1977, 15, 3609.
72. Arratia-Perez, R. Chem Phys Lett 1993, 213, 547.
73. Perdew, J. P.; Levy, M. Phys Rev Lett 1983, 51, 1884.
74. Perdew, J. P. Int J Quantum Chem Symp 1986, 19, 497.